THE UNIVERSITY OF MICHIGAN

RESEARCH INSTITUTE
ANN ARBOR

Final Report

INFLUENCE OF WIND AND ANGLE OF INCIDENT RADIATION ON THE PERFORMANCE OF A BECKMAN AND WHITLEY TOTAL HEMISPHERICAL RADIOMETER

Donald J. Portman
Associate Research Meteorologist

Fleming Dias
Research Assistant

UMRI Project 2715

under contract with:

UNITED STATES DEPARTMENT OF COMMERCE
WEATHER BUREAU
WASHINGTON, D. C.

administered by:

THE UNIVERSITY OF MICHIGAN RESEARCH INSTITUTE ANN ARBOR

April 1959

PREFACE

The work described in this report was conducted under United States Department of Commerce, Weather Bureau, Contract Number Cwb-9350 signed on March 11, 1958. The general purpose of the work was to conduct a series of tests and investigations directed toward the evaluation of the Beckman and Whitley total hemispherical thermal radiometer. This report, giving a description of the tests and a tabulation and summary of the data obtained, constitutes the final, and only, report required under the terms of the contract.

The authors wish to express their appreciation to James Ruffner and Edward Ryznar of the University of Michigan Research Institute for their assistance in the observational phase of this investigation.

TABLE OF CONTENTS

LIST OF TABLES

LIST OF FIGURES

ABSTRACT

A Beckman and Whitley Model H188-01 Total Hemispherical Radiometer was tested in a wind tunnel and in the natural wind to determine the influence of wind speed and direction (relative to radiometer) on the indicated radiation. It was found that for the radiometer sensing element initially warmer than the air the indicated radiation was always less than actual radiation in the presence of wind and that, in general, it decreased with increasing wind speed. Cross winds had the greatest influence. An expression for wind error in indicated radiation is derived making it possible to estimate radiometer error from wind and air temperature data.

The same instrument was tested to determine the influence of angle of incidence on the indicated radiation. Especially large deviations from the cosine law were found for large angles of incidence. These are explained by the shading caused by radiometer structural members surrounding the sensing element.

The results are presented in both tabular and graphical form and the equipment and procedures are described.

Influence of Wind and Angle of Incident Radiation on the Performance of a Beckman and Whitley Total Hemispherical Radiometer

PART I

Influence of Wind

A. Conclusions

1. Wind Tunnel Tests — From the results of wind tunnel tests on a Beckman and Whitley Total Hemispherical Thermal Radiometer (Model H188-01, Ser. 150) it may be concluded that, for the sensing element initially warmer than the air, the influence of a steady wind is to cause the radiometer to indicate less radiation than was actually received. An analysis of the heat balance of the sensing elements shows that for the sensing element initially cooler than the air the radiometer would indicate more radiation than was actually received.

Figure 1 is a composite graph showing curves drawn from the data obtained in wind tunnel tests. The abscissa scale is based on the indicated radiation in the absence of wind. In all cases the radiometer sensing element was initially 3 (±0.3) deg. C. warmer than the air. The indicated radiation decreases steadily with an increase in wind speed except for the case of wind directly opposing the radiometer jet in the region of 25 to 35 mph. Up to 30 mph the radiometer output is least influenced by wind corresponding in direction with the radiometer jet. Between 30 to 50 mph an opposing wind shows least influence.

2. Natural Wind Tests — From limited tests in the natural wind it may be concluded that the influence of natural wind is similar to , but possibly greater than, that produced in the wind tunnel. Turbulence in the natural wind caused the radiometer output to have spurious fluctuations. The fluctuations are smallest for a natural wind corresponding in direction with the radiometer jet and greatest for a natural wind normal to the direction of the radiometer jet.

3. General Conclusions relating to Wind Influence — An analysis of the heat balance of the radiometer sensing element shows that the wind may influence the radiometer performance either (1) by altering the convective heat transfer coefficient, h, without upsetting the equality of the coefficients for the upper and lower surfaces of the sensing element, or (2) by destroying the equality of the upper and lower coefficients. When the coefficients are not equal the radiometer accuracy depends on the difference between the sensing element temperature and the air temperature as well as on the difference between coefficients.

Consideration of the radiometer configuration and the way in which the sensing element and its radiation shield are mounted suggests that almost any wind influence would be associated with an inequality of the upper and lower coefficients. It suggests, further, that the coefficient of the upper surface is much more influenced by the wind than is the coefficient for the lower surface. If it is assumed that only the upper surface coefficient is altered by the wind it is possible to derive a simple expression for radiometer error due to wind influence. It is

$$E' = (h_1 - h)\ (t_m - t_a)$$

in which E' is an approximate error, h_1 is the resulting convective heat transfer coefficient for the upper surface, h the undisturbed coefficient, t_m the temperature of the sensing element and t_a the air temperature. The quantity $(h_1 - h)$ may be determined for different wind speeds and relative directions from the wind tunnel test data. Thus it is possible to correct radiometer data if wind speed, relative wind direction and air temperature are known for the periods of radiation measurement.

The test data and the analysis both indicate that, particularly for winds under 30 mph, the best operating position of the radiometer is for the jet to correspond in direction with the natural wind. For steady wind above 30 mph the wind tunnel tests indicate that the radiometer should be mounted with the jet opposing the wind for least error. Since, however, high natural winds are usually gusty, the validity of this conclusion remains in doubt in light of the conclusions reached concerning the influence of turbulence from the natural wind tests.

Many of the results obtained during this investigation suggest that relatively simple design changes would significantly improve the radiometer performance in natural wind.

B. Results

1. Wind Tunnel Tests — The equipment and procedures used in the wind tunnel tests are described in detail in Appendix A. The radiometer was mounted near the center of the working section of a large wind tunnel. Radiation from a heat lamp above the working section was directed on the radiometer sensing element through a series of apertures and was held constant by control of its power supply. Tunnel air speed was varied from zero to near 50 mph for each of four positions of the radiometer. For each position the initial temperature difference, sensing element temperature minus air temperature, was +3 ($\pm$0.3) deg. C.

Test results for the four radiometer positions are given in Tables I, II, III and IV. Thermopile output and plate temperature data are listed for each wind speed and are combined as indicated to obtain values of the relative response, G_x/G_o. G_x is the total radiation flux indicated at a given wind speed and G_o is the radiation flux with zero wind speed. Each entry was obtained from a steady recording of at least 5 minutes duration. The test results are summarized in the following paragraphs.

a) Corresponding Wind — Wind tunnel test results for the radiometer jet directed down wind are given in Table I and are shown graphically in Figure 2. The data show a steady decrease in indicated radiation with an increase in wind speed to a relative response of 0.882 at 49.1 mph. Between 0 and 20 mph the relative response decreases in a nearly linear fashion to about 0.97 at 20 mph.

b) Opposing Wind — Results of tests with the radiometer jet directed into the wind are given in Table II and are shown graphically in Figure 3. The outstanding feature of this set of data is that the relative response decreases to a minimum of 0.89 at about 24 mph, then increases to 0.98 at about 35 mph and decreases steadily thereafter to 0.909 at about 64 mph. As indicated in Figure 1 the relative response for an opposing wind is not significantly different from that of a corresponding wind from zero to 20 mph. For winds greater than 30 mph, however, the relative response for the opposing wind is greater than for any of the other directions tested.

Between 20 to 30 mph in the opposing wind the radiometer output was actually quite unstable making it difficult to obtain steady readings. Measurements were repeated several times in this region to establish as nearly as possible a curve representing steady conditions.

c) Right Cross Wind — Right cross wind is defined as the relative wind direction occurring when the wind tunnel stream approaches an observer's right side when he is facing the direction to which the radiometer jet is directed. In this reference sense, the radiometer blower intake is on the left side of the instrument. Results of the tests conducted for this position are listed in Table III and graphed in Figure 4.

The data show a uniform decrease in relative response with increasing wind speed quite similar to the results obtained with the corresponding wind. There is a difference in the magnitude, however, for in this case at 20 mph the relative response is about 0.92 and the 20 mph value for a corresponding wind is 0.97. At 49.1 mph the right cross wind relative response is 0.768 while the value for the corresponding wind for the same speed is 0.882. In the region of 22 to 26 mph these results are approximately the same as those obtained for an opposing wind.

d) Left Cross Wind — Left cross wind is defined as the relative wind direction occurring when the wind tunnel stream approaches an observer's left side when he is facing the direction to which the radiometer jet is directed. In this case the wind tunnel stream is directed into the blower intake. Results of this test are given in Table IV and in Figure 5.

From zero to 22 mph the results for this test are almost identical to those obtained for the right cross wind tests. From 22 to near 50 mph, however, the left cross wind relative response data are consistently nearer one than are the right cross wind data. At 49.1 mph the value of the former is 0.827; the latter is 0.768.

2. Natural wind Tests — Equipment and procedures used in the natural wind tests are described in detail in Appendix B. The radiometer was mounted horizontally at about one meter above the ground over a uniform and level, cut grass

surface on the east edge of the Willow Run Airport. The data given in Table V were obtained with a southwest wind and a nearly cloudless sky. Wind speed and direction were measured at radiometer height with a sensitive anemometer and wind vane. The radiometer was rotated on a vertical axis to obtain data for corresponding, opposing, and left cross wind conditions. Since it was not possible to measure the radiation for zero wind speed, only comparative results for the different positions can be presented. The results are further complicated by the fact that the total incoming radiation flux varied in a typical diurnal pattern through the course of the experiment.

The data presented in Table V were obtained on a single day, the only day of several during which tests were attempted that the wind and radiation condition were sufficiently uniform to permit useful analysis of the results. In general the data presented here substantiate the findings of the wind tunnel tests in that the relative response for winds between 6 and 22 mph is less for a cross wind than for an opposing wind and less for an opposing wind than for a corresponding wind. The ratio of indicated radiation for opposing wind to that for corresponding wind is about 0.96 and the similar ratio for cross wind to corresponding wind is about 0.935.

The results must be used with some care since it was obviously necessary to estimate the radiation that would be indicated had the radiometer been positioned for a corresponding relative direction. The estimation was made by plotting pyrheliometer observations along with the radiometer measurements made in the corresponding wind position and then interpolating the latter for periods when the radiometer was in other than a corresponding wind position. Such interpolations are valid only when the wind and radiation conditions are steady relative to the time intervals for which average indications are compared. In spite of the precarious nature of this procedure of analysis it is felt that the results presented here represent radiometer performance in at least a qualitative way.

C. Discussion

1. Wind Tunnel and Natural Wind Tests — To understand the influence of wind on the performance of the total hemispherical radiometer it is necessary to analyze the heat balance of the sensing element. Although an analysis is given in Reference 1 it will be repeated here, with some modification, to isolate the wind influence.

The radiometer sensing element is a flat plate, approximately 4-1/2" x 3-5/8" x 7/64", composed of 5 laminates. The upper surface is coated with a highly absorptive black paint and the under surface is polished aluminum. The exterior laminates are 2/64" thick aluminum and the three interior laminates, each 1/64" thick, are made of a phenolic resin. The central laminate bears a silver-constantan thermopile of several hundred junctions, so arranged that its output is proportional to the temperature difference between the plate surfaces. A small thermocouple junction is imbedded between the center laminate and the laminate just above it.

The plate is centrally positioned in an air stream created by an electric blower-motor. The air is forced through a rectangular orifice about 5" wide and 1/2" high and 1" from the "leading" edge of the sensing element.

An aluminum radiation shield is positioned parallel to and about 1/2" below the sensing element. The side edges of the shield are formed into vertical sections for support. Its inward facing surface is black and its outward face is polished for maximum reflectivity. The sensing element and its shield are supported by side rails extending forward from the nozzle.

To establish a relationship between the various heat transfer terms and the radiometer response, two heat balance equations are formulated. The first one defines the heat balance of the upper black surface:

$$A_1 G_1 = e_1 \sigma T_1^4 + h_1 (t_1 - t_a) + (K/L) (t_1 - t_2) \qquad (1)$$

in which

A_1 = Absorptivity of the black receiving surface, dimensionless;

G_1 = Total incident energy on the black receiving surface, ly/min;

σ = Stephan-Boltzman constant, ly/min./ (deg. K)^4

e_1 = Emissivity of the black receiving surface, dimensionless;

T_1 = Temperature of the black receiving surface, deg. K;

h_1 = Convective heat transfer coefficient at the black receiving surface, ly/min. deg;

t_1 = Temperature of the black receiving surface, deg. C;

t_a = Temperature of ambient air, deg. C;

K = Thermal conductivity of sensing element, ly cm/min. deg. C;

L = Thickness of sensing element, cm.;

t_2 = Temperature of the polished surface, deg. C;

A similar equation for the lower surface of the sensing element is

$$A_2 G_2 = e_2 \sigma T_2^4 + h_2 (t_2 - t_a) - (K/L) (t_1 - t_2) \qquad (2)$$

Definition of a convective heat transfer coefficient, h, implies that fully forced convection exists with negligible heat transfer by buoyancy effects. The coefficient is assumed to be independent of the temperature difference between the plate surface and the air, but for a fixed shape and size of sensing element, it will depend on the mean speed of the air stream.

Following the development in Reference 1 it may be assumed, with close approximation, that $A_2 G_2 \approx e_2 \sigma T_2^4$. The assumption is based on the fact that

the lower surface of the sensing element and the upper surface of the radiation shield (the source of G_2) are at nearly the same temperature. In addition, A_2 and e_2 are small because the surface is polished metal.

Equation (2) reduces then to

$$h_2 (t_2 - t_a) = (K/L) (t_1 - t_2) \tag{3}$$

Subtracting (3) from (1), rearranging and assuming that $A_1 = e_1 = e$ for the black surface gives

$$e G_1 = e\sigma T_1^4 + h_1 (t_1 - t_a) - h_2 (t_2 - t_a) + (2K/L) (t_1 - t_2) \tag{4}$$

The quantity $e\sigma T_m^4$, in which T_m is the temperature (in degrees K) measured with the imbedded thermocouple junction, may be subtracted from both sides giving

$$e G_1 - e\sigma T_m^4 = e\sigma (T_1^4 - T_m^4) + h_1 (t_1 - t_a) - h_2 (t_2 - t_a) + (2K/L) (t_1 - t_2) \tag{5}$$

Since the difference $T_1 - T_m$ is always very small

$$T_1^4 - T_m^4 \approx 4 T_m^3 (T_1 - T_m) \tag{6}$$

Because T_m is measured at a fixed point between the upper and lower plate surfaces of the sensing element, the difference between T_1 and T_m is a constant fraction of $(T_1 - T_2)$ or $(t_1 - t_2)$ for steady conditions. Nearly steady conditions may be assumed to exist at all times because of the small heat capacity of the sensing element. Thus

$$T_1 - T_m = b (t_1 - t_2) \tag{7}$$

in which b is an unknown constant.

In Reference 1 it is assumed that $b = 1/3$, an appropriate value if the thermal resistance of the aluminum cover plates is negligible with respect to that of the phenolic resin laminates. Substitution of (7) with $b = 1/3$ in (6) gives

$$(T_1^4 - T_m^4) = (4/3) T_m^3 (t_1 - t_2) \tag{8}$$

and (5) can be written

$$G_1 - \sigma T_m^4 = \left[(4/3)\sigma T_m^3 + (2K/eL)\right] (t_1 - t_2) + (h_1/e) (t_1 - t_a) - (h_2/e)(t_2 - t_a) \tag{9}$$

If it is now assumed that $h_1 = h_2 = h$, (9) reduces to

$$G_1 - \sigma T_m^4 = \left[(4/3)\sigma T_m^3 - (2K/eL) + (h/e)\right] (t_1 - t_2) \tag{10}$$

which is the relationship derived in Reference 1.

Since the radiometer thermopile output is proportional to $(t_1 - t_2)$ for steady conditions, (10) may be written

$$G_1 = k\ (mv) + \sigma T_m^4 \qquad (11)$$

if the quantity in parentheses in (10) is constant. Equation (11) is the relationship used to determine G_1 from measurement of (mv) and T_m. The constant, k, is determined by calibration.

Comparison of (9) and (10) shows that if, and only if,

$$h\ (t_1 - t_2) = h_1\ (t_1 - t_a) - h_2\ (t_2 - t_a) \qquad (12)$$

will the radiometer yield correct measurements according to its calibration.

Equation (12) is satisfied, of course, if $h_1 = h_2 = h$. This special case was explored to determine the effect of variations in h on the radiometer output. The method was to decrease the speed of the blower motor while exposing the radiometer to a steady radiation flux. It was assumed that h_1 and h_2 were equal regardless of the jet speed. The experiment was conducted with the radiometer in both upright and inverted positions to ascertain any possible influence of buoyancy in the convective heat transfer. The results of the tests are given in Table VI.

TABLE VI

Radiometer Test Data for Variation of Convective Heat Transfer Coefficent

		Upright				Inverted			
1.	2.	3.	4.	5.	6.	7.	8.	9.	10.
v	mph	t_a	t_m	mv	G	t_a	t_m	mv	G
112	26	23.2	33.4	26.4	3.542	23.0	32.3	25.4	3.426
100	25	23.2	33.0	26.2	3.517	23.4	32.2	25.2	3.403
90	23	23.4	33.6	26.3	3.534	23.2	33.0	25.6	3.453
70	9	23.4	36.8	27.5	3.693	23.2	35.4	26.5	3.572

Key

1.	v	Voltage applied to blower motor, volts.
2.	mph	Air speed measured over sensing element, mph.
3., 7.	t_a	Air temperature, deg. C.
4., 8.	t_m	Temperature of radiometer sensing element, deg. C.
5., 9.	mv	Output of thermopile, millivolts.
6., 10.	G	Total radiation indicated by radiometer, ly/min.

The air speeds reported in Table VI were obtained with an Alnor Velometer by placing the probe intake, an oval orifice 3/16" by 1/2", at the center of the sensing element. The air temperatures were measured with a fine-wire thermocouple junction placed inside the radiometer blower nozzle, about 1/2 inch from the orifice. The data show an increase in thermopile output of 4.2 and 4.3 percent for upright and inverted positions respectively, for a change in air speed from 26 to 9 mph. Parekh (Reference 2) has given data on the variation of heat transfer coefficients with air speed for a flat plate 3" x 2" x 1/8" with a blunt leading edge. His data show a decrease in heat transfer coefficient of about 42 percent for a velocity change of from about 30 mph to 10 mph. The latter values apply approximately to the leading edge, center, of the sensing element for blower motor voltages of 112 and 70, respectively.

In Reference 1 numerical values were established for each of the terms inside the bracket in Equation (9). If these values are adopted it is found that the term h/e accounts for about 10 percent of the sum of all the terms. Thus a 42 percent change in h would be expected to cause only 4.2 percent change in indicated radiation if $e = 1$. The very close agreement between this value and the measured 4.3 percent is probably fortuitous but the results suggest that equation (11) applies and that small variations in h do not cause serious errors in indicated radiation.

The data in Table VI indicate, further, that buoyancy effects are probably not significant, even for aspiration rates as low as 9 mph. This may be concluded from the fact that equal changes in air velocity in the two positions yielded nearly identical changes in indicated radiation.

Because of the configuration of the radiometer and the way in which the sensing element is mounted it seems likely that much of the observed wind influence may be associated with an inequality of h_1 and h_2. Equation (12) shows that an increase in h_1 relative to h_2, for given positive temperature differences, would result in an effective increase in the term $h(t_1 - t_2)$. Since the data in Table VI show that indicated radiation is inversely related to $h(t_1 - t_2)$, the wind tunnel test results suggest that the cause of the observed general decrease of indicated radiation with increasing wind speed can be accredited to an increase of h_1 relative to h_2.

Cross winds show the greatest effect. This would be expected from the foregoing analysis since the lower surface of the sensing element is protected from cross winds by the vertical sections of the radiation shield. Opposing wind shows the least effect for winds greater than 30 mph. Again, this could be predicted on the basis of the above reasoning since the forward edge of the sensing element and its support offer less obstruction to oncoming wind for both sides of the sensing element than does any other edge. The dip in the relative response curve in the 20 to 30 mph region might be explained by near stagnation conditions in the restricted region between the sensing element and its shield since the normal jet speed over the plate is on the order of 25 mph.

For $h_1 \neq h_2$, the error in indicated radiation may be expressed as the difference between the two sides of Equation (12). That is

$$\text{Error} \quad E = h_1 (t_1 - t_a) - h_2 (t_2 - t_a) - h (t_1 - t_2) \tag{13}$$

or

$$E = t_1 (h_1 - h) - t_2 (h_2 - h) - t_a (h_1 - h_2)$$

If it is now assumed that the wind modifies the radiometer jet mainly by altering h_1 and that $h_2 \approx h$

then

$$E \approx (h_1 - h) (t_1 - t_a) .$$

or, since $(t_1 - t_m)$ is very small compared to $(t_1 - t_a)$

$$E' = (h_1 - h) (t_m - t_a) . \tag{14}$$

in which E' is an approximate error

Equation (14) may be used to apply the wind tunnel test data in correcting radiometer recordings when wind and air temperature data are available. For example, for corresponding wind between 25 and 50 mph the test data (Table I) show that E varied from 0.075 to 0.152 ly/min while $(t_m - t_a)$ remained constant at about $2^{\circ}C$. Thus it may be concluded that $(h_1 - h)$ varied from 0.038 to 0.076 in a very nearly linear fashion. Therefore, the corrections could be determined simply by multiplying observed temperature differences, $(t_m - t_a)$, by the appropriate value of $(h_1 - h)$ as determined according to the measured wind speed.

It should be noted that E' (and E) will change sign for $t_a > t_m$, which is the case for typical nighttime operation. This should not, however, reduce the validity of Equation (14).

Verification of Equation 14 by wind tunnel testing could not be achieved because of limitations in both project funding and availability of the wind tunnel during the period authorized for direct effort on the testing program.

TABLE I

WIND TUNNEL TEST DATA: CORRESPONDING WIND

WIND VELOCITY m.p.h	THERMOPILE OUTPUT $(gm\text{-}cal)(cm)^{-2}(min)^{-1}$	PLATE TEMP. °C	σT^4 $(gm\text{-}cal)(cm)^{-2}(min)^{-1}$	$G_x = Kv + \sigma T^4$ $(gm\text{-}cal)(cm)^{-2}(min)^{-1}$	$\frac{G_x}{G_o}$
0	0.618	26.7	0.667	G_o = 1.285	1.000
8.0	0.612	26.2	0.662	1.274	0.991
12.7	0.612	26.0	0.660	1.272	0.990
16.7	0.603	25.7	0.658	1.261	0.981
22.0	0.592	25.7	0.658	1.250	0.973
	AIR TEMPERATURE: 23.4 (± 0.3) deg. C.				
0	0.629	25.5	0.656	1.285	1.000
26.6	0.565	24.3	0.645	1.210	0.942
30.7	0.565	24.3	0.645	1.210	0.942
35.4	0.554	24.3	0.645	1.199	0.933
39.5	0.535	24.3	0.645	1.180	0.918
44.3	0.506	24.3	0.645	1.151	0.896
49.1	0.488	24.3	0.645	1.133	0.882
	AIR TEMPERATURE: 22.2 (± 0.2) deg. C.				

K = calibration constant

$= 0.1066\ (gm\text{-}cal.)(cm.)^{-2}(min.)^{-1} / mv$

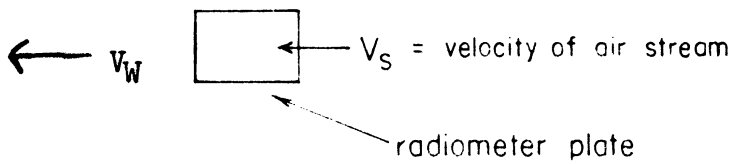

TABLE II
WIND TUNNEL TEST DATA: OPPOSING WIND

WIND VELOCITY m.p.h	THERMOPILE OUTPUT $(gm\text{-}cal)(cm)^{-2}(min)^{-1}$	PLATE TEMP °C	σT^4 $(gm\text{-}cal)(cm)^{-2}(min)^{-1}$	$G_x = Kv + \sigma T^4$ $(gm\text{-}cal)(cm)^{-2}(min)^{-1}$	$\frac{G_x}{G_o}$
0	0.603	26.2	0.662	G_o = 1.275	1.000
8.0	0.597	26.0	0.660	1.257	0.986
12.7	0.589	26.0	0.660	1.250	0.980
16.7	0.582	25.7	0.658	1.240	0.973
22.0	0.522	25.7	0.658	1.180	0.925
	AIR TEMPERATURE: 23.2 (+ 0.2) deg. C.				
0	0.618	26.2	0.662	1.280	1.000
20.8	0.565	25.7	0.658	1.223	0.955
22.3	0.506	25.5	0.656	1.162	0.908
24.5	0.488	25.5	0.656	1.144	0.894
26.2	0.513	25.5	0.656	1.169	0.913
22.3	0.506	25.7	0.658	1.164	0.909
	AIR TEMPERATURE: 23.2 (+ 0.2) deg. C.				
0	0.597	26.2	0.662	1.259	1.000
26.6	0.506	25.5	0.656	1.162	0.923
30.0	0.531	25.5	0.656	1.187	0.943
35.4	0.581	25.2	0.653	1.234	0.980
40.6	0.565	24.7	0.649	1.214	0.964
45.3	0.554	24.7	0.649	1.203	0.956
48.8	0.546	24.7	0.649	1.195	0.949
	AIR TEMPERATURE: 23.5 (+ 0.3) deg. C.				
0	0.618	26.5	0.665	1.283	1.000
63.8	0.514	25.0	0.652	1.166	0.909

AIR TEMPERATURE 23.4 @ 0 mph, 24.4 @ 63.8 mph

K = calibration constant

$= 0.1066\ (gm\text{-}cal.)(cm.)^{-2}(min.)^{-1} / mv$

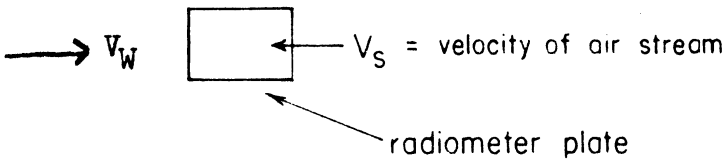

TABLE III

WIND TUNNEL TEST DATA: RIGHT CROSS WIND

WIND VELOCITY m.p.h	THERMOPILE OUTPUT $(gm\text{-}cal)(cm)^{-2}(min)^{-1}$	PLATE TEMP. °C	σT^4 $(gm\text{-}cal)(cm)^{-2}(min)^{-1}$	$G_x = Kv + \sigma T^4$ $(gm\text{-}cal)(cm)^{-2}(min)^{-1}$	$\frac{G_x}{G_o}$
0	0.608	26.70	0.667	G_o = 1.275	1.000
8.0	0.554	26.20	0.661	1.215	0.953
12.7	0.554	26.00	0.660	1.204	0.944
16.7	0.528	25.70	0.660	1.188	0.932
22.0	0.514	25.70	0.660	1.174	0.921
26.6	0.466	24.30	0.643	1.109	0.870
30.7	0.458	24.30	0.643	1.101	0.864
35.4	0.426	24.30	0.643	1.069	0.838
39.5	0.400	24.30	0.643	1.043	0.818
44.3	0.362	24.30	0.643	1.005	0.788
49.1	0.336	24.30	0.643	0.979	0.768
	0-22 mph	**AIR TEMPERATURE**	**23.4**	**(± 0.2) deg. C.**	
	26.6-49.1 mph	**AIR TEMPERATURE**	**22.0**	**(± 0.2) deg. C.**	

K = calibration constant

$= 0.1066\ (gm\text{-}cal.)(cm.)^{-2}(min.)^{-1} / mv$

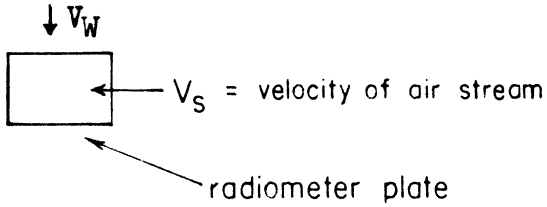

TABLE IV

WIND TUNNEL TEST DATA: LEFT CROSS WIND

WIND VELOCITY m.p.h	THERMOPILE OUTPUT $(gm\text{-}cal)(cm)^{-2}(min)^{-1}$	PLATE TEMP. °C	σT^4 $(gm\text{-}cal)(cm)^{-2}(min)^{-1}$	$G_x = Kv + \sigma T^4$ $(gm\text{-}cal)(cm)^{-2}(min)^{-1}$	$\frac{G_x}{G_o}$
0	0.613	26.7	0.666	G_o = 1.279	1.000
8.0	0.565	26.2	0.662	1.227	0.959
12.7	0.554	26.0	0.660	1.214	0.949
16.7	0.537	25.7	0.658	1.195	0.934
22.0	0.533	25.7	0.658	1.191	0.931
	AIR TEMPERATURE 23.4 (±0.2) deg. C.				
0	0.597	25.5	0.656	1.253	1.000
23.9	0.506	24.6	0.648	1.154	0.921
26.6	0.580	24.4	0.646	1.126	0.899
30.7	0.464	24.3	0.645	1.109	0.885
35.4	0.426	24.3	0.645	1.071	0.855
39.6	0.411	24.3	0.645	1.056	0.843
44.3	0.394	24.3	0.645	1.039	0.829
49.1	0.391	24.3	0.645	1.036	0.827
	AIR TEMPERATURE 22.3 (±0.3) deg. C.				

K = calibration constant

$= 0.1066\ (gm\text{-}cal.)(cm.)^{-2}(min.)^{-1} / mv$

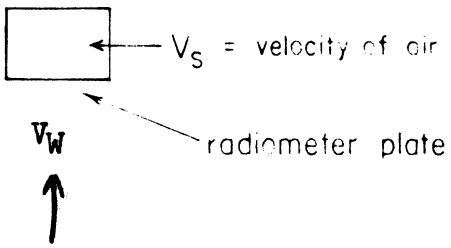

TABLE V

DATA FROM RADIOMETER TESTS IN NATURAL WIND

1 Period	2. U	3. U_{min}	4. U_{max}	5. WD_r	6. G_s	7. t_a	8. t_m	9. G	10. G_i	11. G/G_i	12. Rel. Direct
1143-1153	12.5	6.0	18.7	76	1.34	26.8	35.8	2.09	2.17	0.96	Opposing
1154-1202	11.3	6.0	17.8	88	1.42	27.0	35.9	2.17	---	---	Corresponding
1332-1342	11.8	6.0	18.5	80	1.20	27.8	36.3	1.96	2.08	0.94	Left cross
1346-1356	11.5	6.0	19.7	88	1.30	27.8	36.7	2.06	---	---	Corresponding
1358-1408	11.3	6.0	18.7	81	1.19	28.0	36.9	1.95	2.03	0.96	Opposing
1426-1437	14.1	7.4	19.9	80	1.13	28.4	36.4	1.89	1.96	0.96	Opposing
1526-1536	13.4	7.7	22.6	55	1.00	28.7	36.1	1.75	---	---	Corresponding
1543-1553	14.2	7.9	22.1	60	0.81	28.3	35.6	1.56	1.68	0.93	Left cross
1600-1610	13.2	7.9	20.2	87	0.79	28.2	35.4	1.53	1.62	0.95	Opposing

Key:

1. Period — Time period of observations, EST.
2. U — Average wind speed, mph.
3. U_{min} — Minimum wind speed indicated, mph.
4. U_{max} — Maximum wind speed indicated, mph.
5. WD_r — Range of wind direction, degrees.
6. G_s — Average total incoming solar radiation, ly per min.
7. t_a — Average air temperature at 1 meter above ground, deg. C.
8. t_m — Average temperature of radiometer sensing element, deg. C.
9. G — Total radiation indicated by radiometer, ly/min.
10. G_i — Estimated value of radiation that would be indicated had the radiometer been in a corresponding wind position, ly/min.

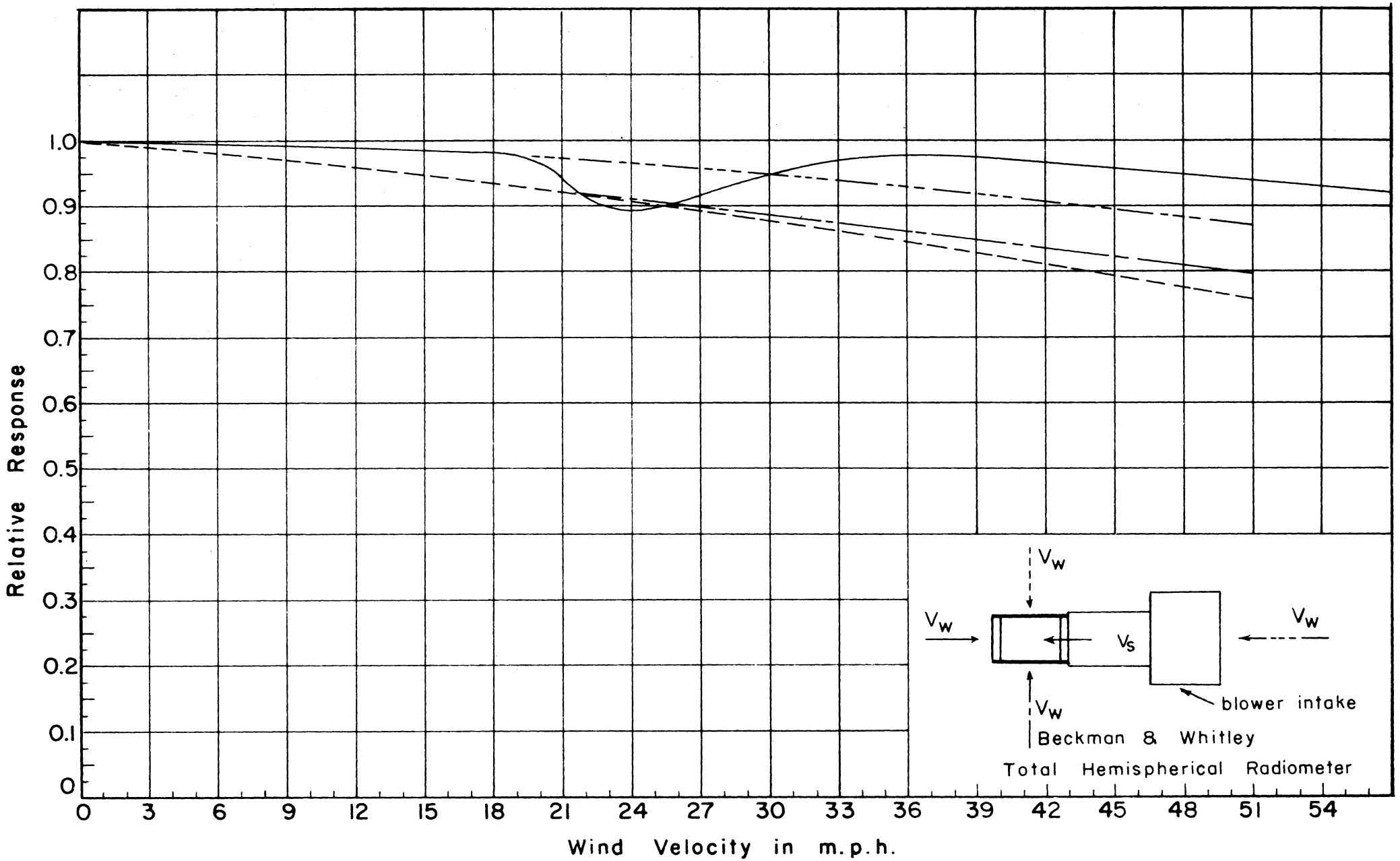

Fig. 1 INFLUENCE OF WIND VELOCITY ON RADIOMETER RESPONSE

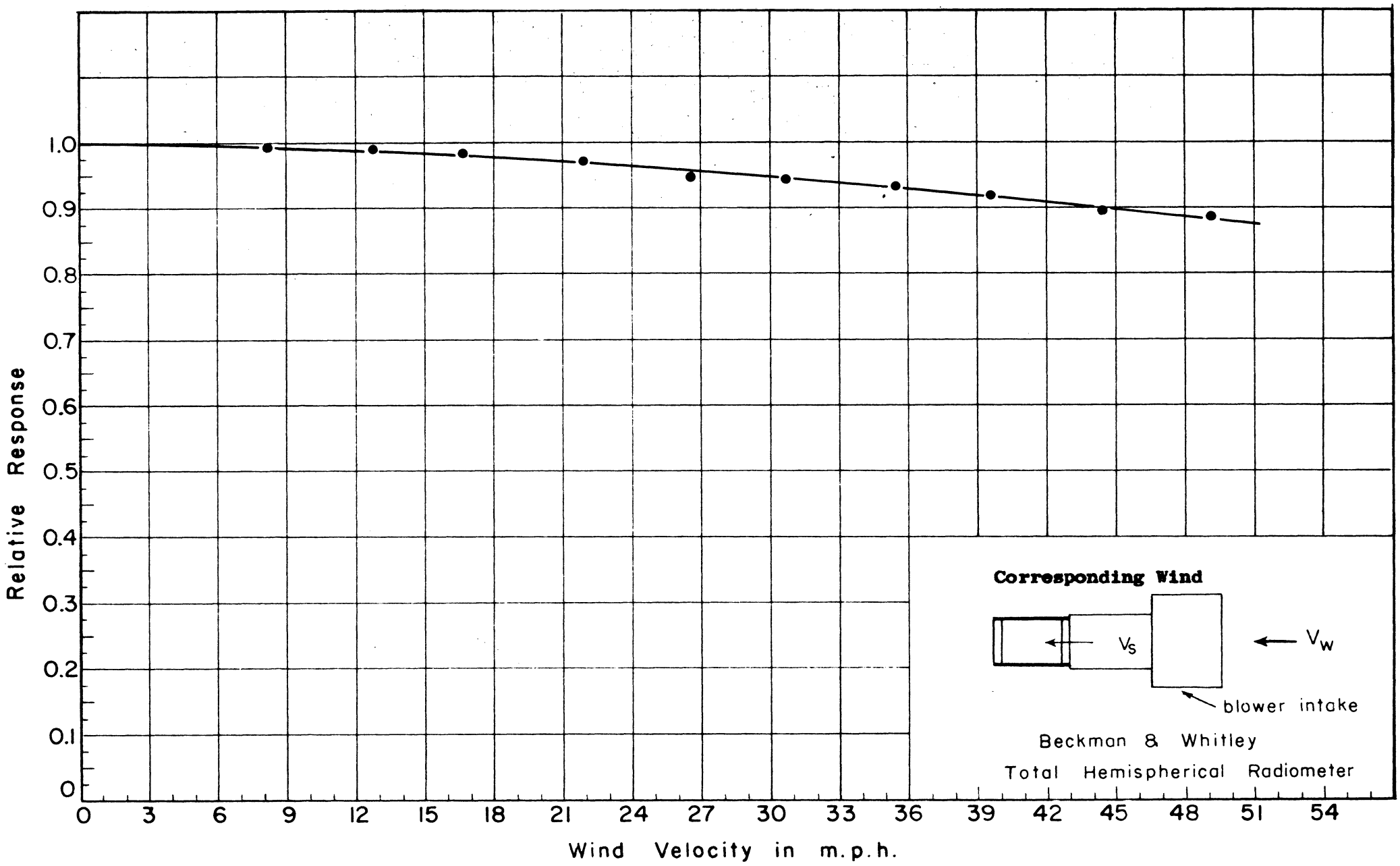

Fig. 2 INFLUENCE OF WIND VELOCITY ON RADIOMETER RESPONSE

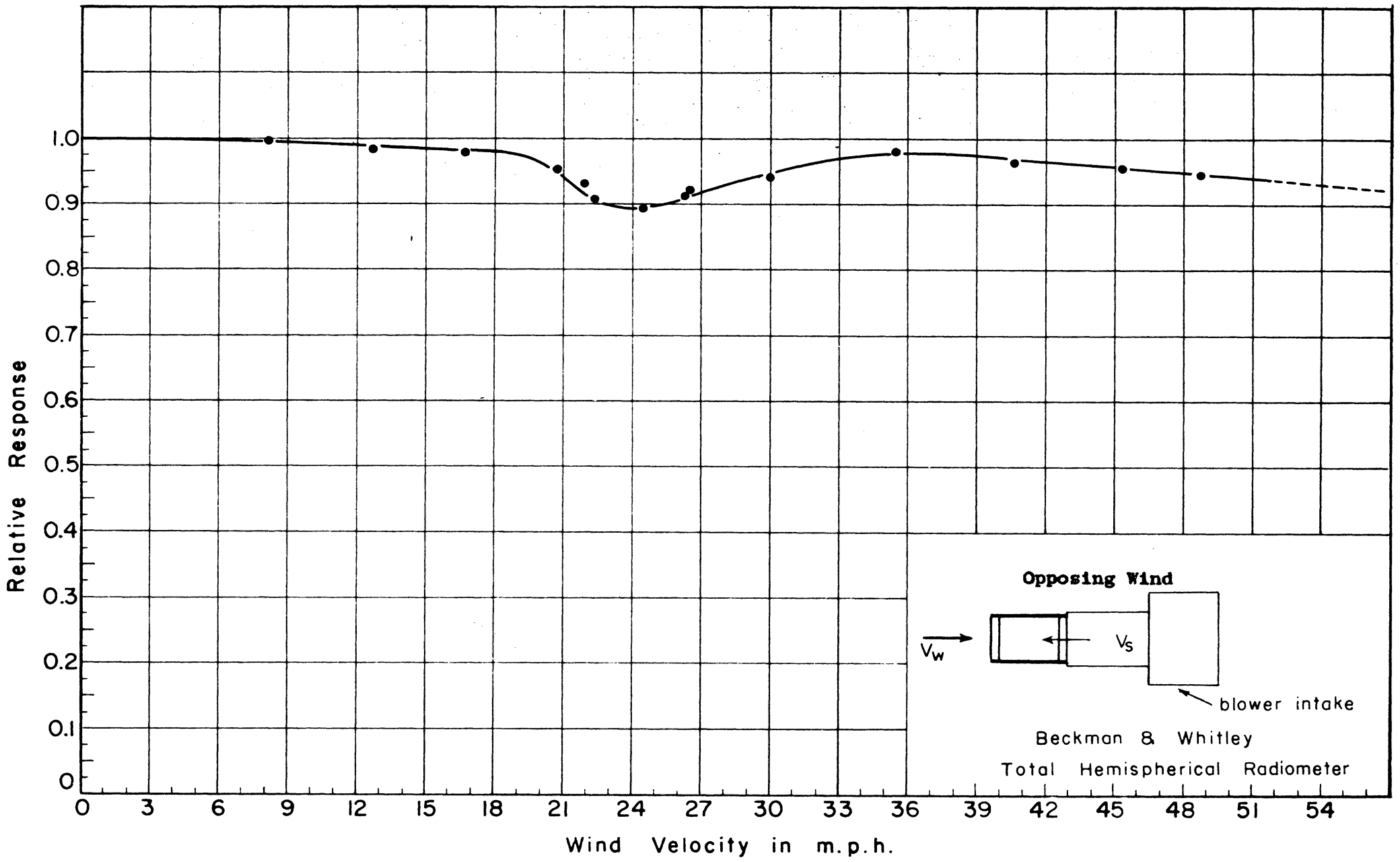

Fig. 3 INFLUENCE OF WIND VELOCITY ON RADIOMETER RESPONSE

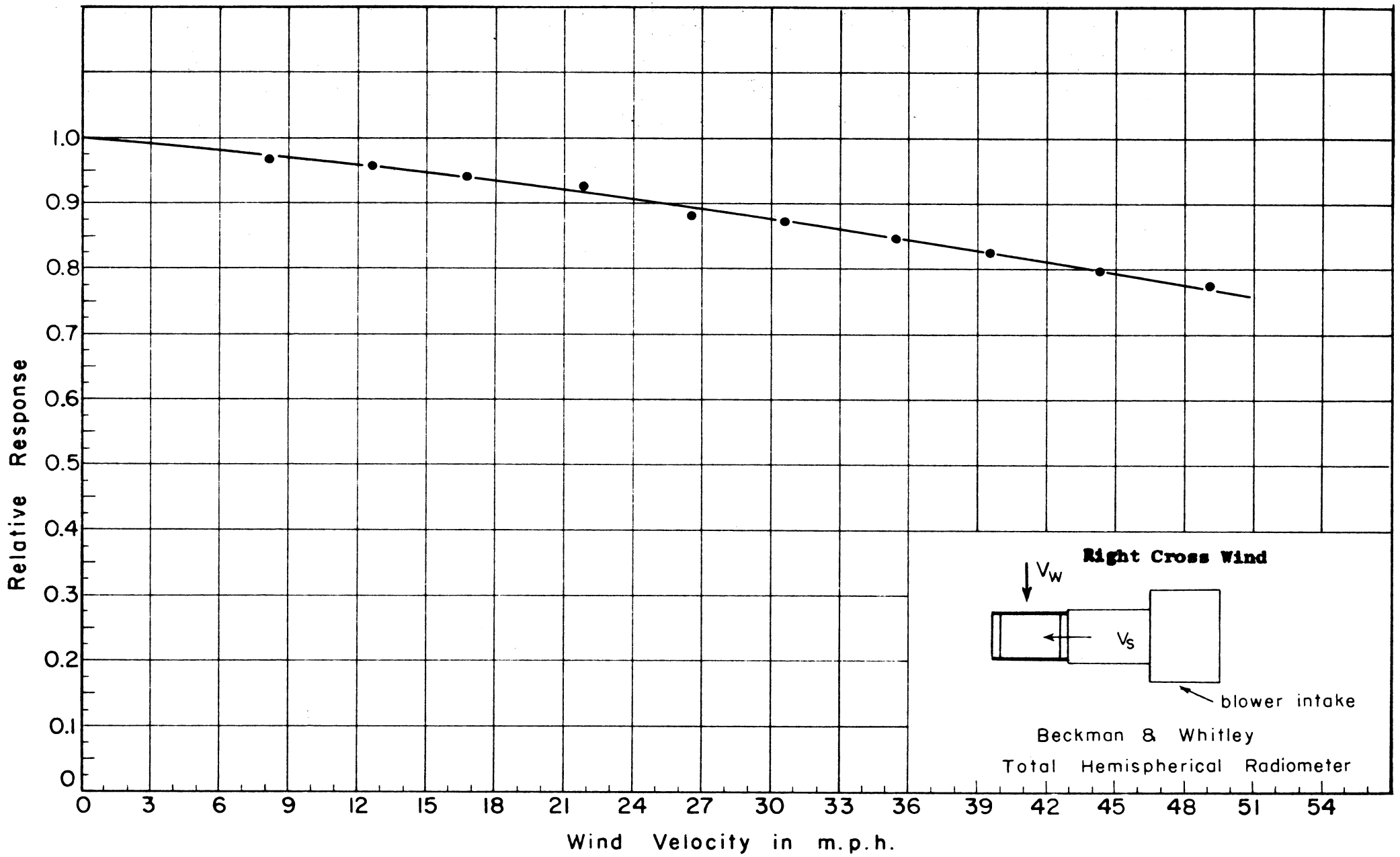

Fig. 4 INFLUENCE OF WIND VELOCITY ON RADIOMETER RESPONSE

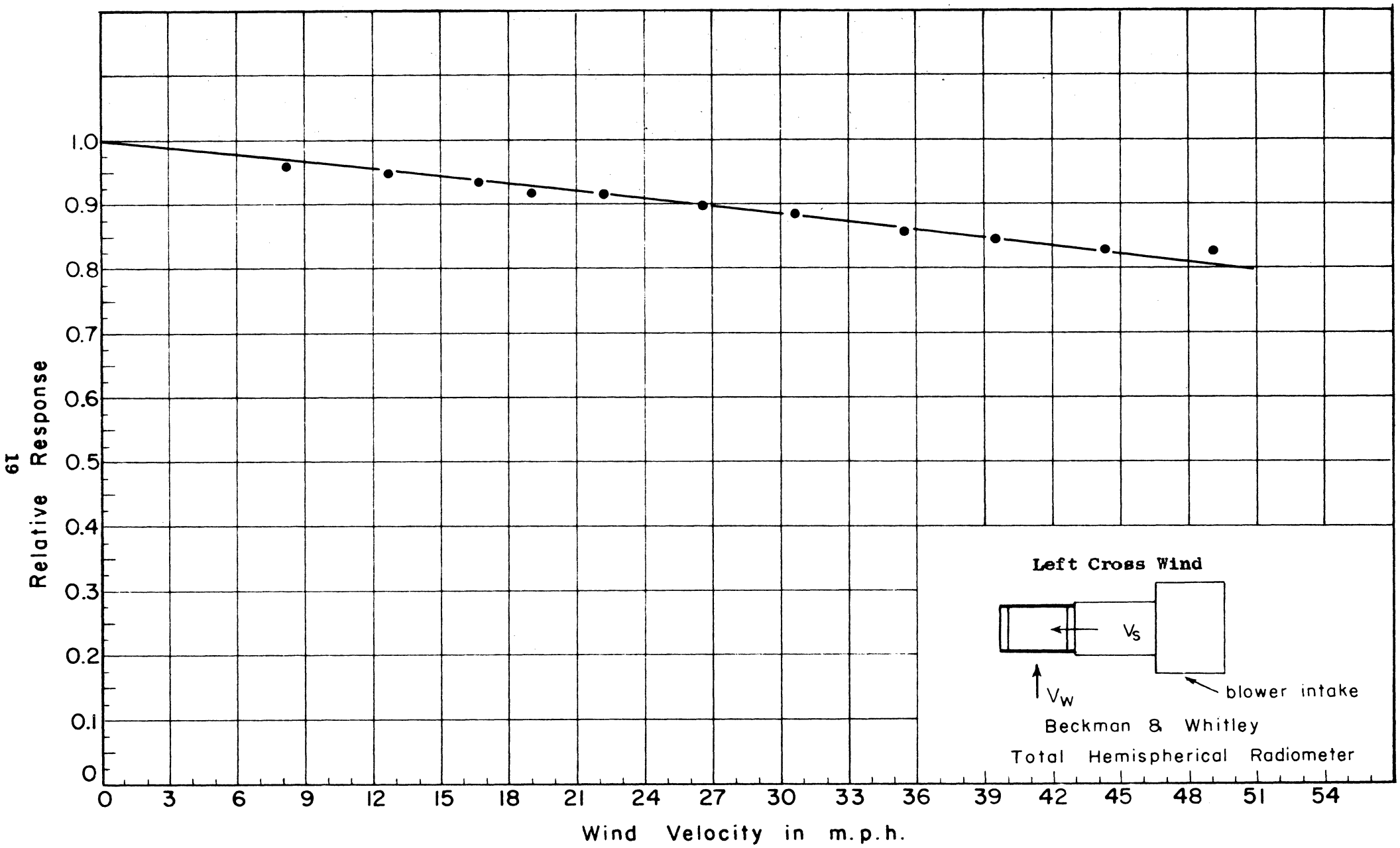

Fig. 5 INFLUENCE OF WIND VELOCITY ON RADIOMETER RESPONSE

PART II

Influence of Angle of Incident Radiation

A. Conclusions

Tests of the influence of angle of incident radiation on the radiometer output indicate that, on the average, there is less than one percent deviation from the cosine law for angles between 0 and 50 degrees measured from normal incidence. The average deviation increases from about 1 percent at 50 degrees to nearly four percent at 70 degrees. At 80 degrees the average deviation is on the order of 20 percent. The averages were determined from algebraic sums of six separate measurements involving three axes of revolution. It appears that shadows cast by the end of the nozzle and the structure supporting the plate are mainly responsible for large deviations from the cosine law for angles greater than 70 degrees.

B. Results

The equipment and procedures used in the cosine response tests are described in detail in Appendix C. The arrangement consisted of the radiometer mounted on the base of a Warner and Swasey Azimuth Instrument with the radiometer sensing element in a vertical plane. Radiation from a photo spot lamp was directed on the radiometer through a series of apertures and was held constant by control of its power supply. The radiometer was rotated about a vertical axis and steady recordings of radiometer output were made at 10 degree intervals with the light beam (1) incident on the sensing element, and (2) interrupted by a shutter on one of the apertures. The radiometer was arranged in three different positions on the azimuth instrument base to obtain three different axes of revolution relative to the radiometer. The test equipment and its arrangement are shown in Figures 13, 14, and 15.

The test results are summarized in Table VII in the form of computed deviations from the cosine law in percent of $G_2 \cos \theta$. The angle of incidence, θ, is measured from $\theta \simeq 0$ at normal incidence. G_2 is the measured parallel beam radiation at normal incidence. The three axes, a-a, b-b, c-c, are defined in the radiometer diagrams in Figures 6, 7, and 8. The curved arrow in each diagram indicates a counterclockwise rotation.

The polar graphs in Figures 6, 7, and 8 show the test results for the different axes of rotation with respect to a circle representing complete fulfillment of the cosine law. The right side of each graph shows data for counterclockwise rotation and the left side for clockwise rotation.

Detailed experimental data and various computational procedures are shown in Tables VIII, IX, and X. It should be noted that it was necessary to eliminate the background fluxes $(K_{nb} + T_{nb}^4)$ and $(K_{\theta b} + T_{\theta b}^4)$ in order to compute the cosine response, G_1/G_2.

TABLE VII

Observed Deviations from the Cosine Law in Percent of G_2 Cos θ

	1) Counterclockwise rotation				2) Clockwise rotation			
0	10°	20°	30°	40°	50°	60°	70°	80°
Axis a-a								
1)	1.3	0.3	-1.7	-2.5	-4.0	-7.0	-11.6	-38.5
2)	0.9	0.6	-0.1	1.6	0.2	-1.4	-5.0	-13.8
Axis b-b								
1)	0.4	0.6	0.9	1.3	1.2	-2.2	-5.3	-43.7
2)	0.9	-1.1	-0.2	-2.0	-2.6	-2.4	-0.3	-13.8
Axis c-c								
1)	0.1	0.6	0.6	1.2	1.6	0.4	1.5	-9.2
2)	-1.8	-2.3	-0.6	-2.4	-1.9	-1.8	-2.6	-7.5
Average								
	0.3	-0.2	-0.2	-0.5	-0.9	-2.4	-3.9	-21.1

C. Discussion

The cosine response test results as shown in Table VII reveal both positive and negative deviations for incidence angles of 70 degrees and less. At 80 degrees all deviations are negative. For angles below 70 degrees the results are difficult to explain because most of the deviations are small--all but three of the 36 observations are less than 2.5 percent. Quite likely, experimental error accounts for much of the deviation observed for this group of data. On the other hand, paint characteristics or non-uniformity in the plate surface could easily account for the results. Fuquay and Buettner (Reference 3) measured the cosine response characteristics for five pyrheliometers and found deviations as large as -7 percent at 70 degrees. (They also tested the paint used on the Beckman and Whitley radiometers but reported merely that it appeared to be superior to other blackening agents with respect to "blackness" and cosine response.) Since there appears to be little, if any, systematic pattern to the findings for the separate axes of rotation for angles less than 70 degrees, one is inclined to attribute most of the variation to experimental error.

The average of the results for all three axes of revolution, however, shows a systematic change from a positive 0.3 percent deviation at 10 degrees to a negative 3.9 percent at 70 degrees. This is the order of deviation that might be expected for a typically "black" surface and may well represent the true cosine response for the painted surface of the sensing element.

The results for 80 degrees must be interpreted in terms of the shading caused by the end of the blower nozzle and the structure supporting the plate. During rotation about axis a-a the shadow caused by a side rail reaches the center of the sensing element at an angle of incidence of 85 degrees. The relatively large deviations observed for axis a-a for angles of 70 and 80 degrees are undoubtedly caused by this effect. The change in output as the shadow spreads across the plate cannot be estimated directly because there are four separate thermopiles symmetrically spaced in the sensing element.

Similar conclusions can be made concerning the results for b-b. The shadow caused by the edge of the nozzle reaches the center of the sensing element at about 82 degrees. At greater angles the shadow of the handle (on the main body of the instrument) extends beyond the nozzle shadow. The cross member joining the side rails at their extremities casts a shadow that reached the center of the sensing element at an angle of about 86 degrees. Thus the large deviations observed for axis b-b at 80 degrees can also be explained by shadow effects.

The deviations observed at 80 degrees for axis c-c are significantly less than the corresponding deviations for the other two axes of revolution. This may be explained by the fact that at 80 degrees, although there is more shadowed area than for the other two cases, it is distributed along two edges thereby producing less influence on the thermopiles.

Perhaps the most important conclusion is that the cosine response could be improved significantly for large angles of incidence by making relatively small changes in the design of the radiometer.

TABLE VIII

COSINE RESPONSE TEST DATA: ROTATION ABOUT AXIS A-A
(Note: Subscript "b" refers to background flux)

Counterclockwise

Angle of Incidence $\Phi°$	Thermopile Output at Normal Incidence (K_n) $K_n = (K'_n - K_{nb})$	Thermopile Output at $\Phi°$ Incidence (K_Φ) $K_\Phi = (K'_\Phi - K_{\Phi b})$	σT_Φ^4	$\sigma T_{\Phi b}^4$	$G_1 = K_\Phi + \sigma(T_\Phi^4 - T_{\Phi b}^4)$	$G_2 = K_n + \sigma(T_n^4 - T_{nb}^4)$	$G_1 \div G_2$	COS Φ
0 normal	0.497	0.497	0.664	0.651	0.510	0.510	1.000	1.000
10	0.497	0.496	0.664	0.651	0.509	0.510	0.998	0.985
20	0.496	0.465	0.666	0.651	0.480	0.509	0.943	0.940
30	0.492	0.419	0.662	0.651	0.430	0.505	0.851	0.866
40	0.501	0.374	0.661	0.651	0.384	0.514	0.747	0.766
50	0.501	0.308	0.658	0.649	0.317	0.514	0.617	0.643
60	0.501	0.233	0.655	0.649	0.239	0.514	0.465	0.500
70	0.501	0.152	0.653	0.649	0.156	0.514	0.304	0.342
80	0.501	0.055	0.649	0.649	0.055	0.514	0.107	0.174
90	0.501	0.000	0.649	0.649	0.000	0.514	0.000	0.000
$\sigma T_n^4 = 0.664$ and $\sigma T_{nb}^4 = 0.651$								

Clockwise

0	0.504	0.504	0.676	0.662	0.518	0.518	1.000	1.000
10	0.504	0.501	0.674	0.660	0.515	0.518	0.994	0.985
20	0.504	0.476	0.674	0.660	0.490	0.518	0.946	0.940
30	0.504	0.435	0.673	0.660	0.448	0.518	0.865	0.866
40	0.503	0.391	0.670	0.659	0.402	0.517	0.778	0.766
50	0.503	0.323	0.669	0.659	0.333	0.517	0.644	0.643
60	0.499	0.245	0.667	0.659	0.253	0.513	0.493	0.500
70	0.496	0.161	0.664	0.659	0.166	0.510	0.325	0.342
80	0.501	0.075	0.662	0.660	0.077	0.515	0.150	0.174
90	0.501	0.000	0.662	0.662	0.000	0.515	0.000	0.000
$\sigma T_n^4 = 0.676$ and $\sigma T_{nb}^4 = 0.662$								

TABLE IX

COSINE RESPONSE TEST DATA: ROTATION ABOUT AXIS B-B
(Note: Subscript "b" refers to background flux)

Counterclockwise

Angle of Incidence $\phi°$	Thermopile Output at Normal Incidence (K_n) $K_n = (K'_n - K_{nb})$	Thermopile Output at $\phi°$ Incidence (K_ϕ) $K_\phi = (K'_\phi - K_{\phi b})$	σT_ϕ^4	$\sigma T_{\phi b}^4$	$G_1 = K_\phi + \sigma(T_\phi^4 - T_{\phi b}^4)$	$G_2 = K_n + \sigma(T_n^4 - T_{nb}^4)$	$G_1 \div G_2$	$\cos \phi$
0 normal	0.515	0.515	0.674	0.658	0.531	0.531	1.000	1.000
10	0.518	0.514	0.672	0.658	0.528	0.534	0.989	0.985
20	0.517	0.491	0.672	0.659	0.504	0.533	0.946	0.940
30	0.524	0.459	0.672	0.659	0.472	0.540	0.874	0.866
40	0.523	0.407	0.671	0.660	0.418	0.539	0.776	0.766
50	0.522	0.341	0.669	0.660	0.350	0.538	0.651	0.643
60	0.522	0.258	0.666	0.661	0.263	0.538	0.489	0.500
70	0.521	0.170	0.665	0.661	0.174	0.537	0.324	0.342
80	0.524	0.053	0.662	0.662	0.053	0.540	0.098	0.174
90	0.524	0.000	0.662	0.662	0.000	0.540	0.000	0.000
$\sigma T_n^4 = 0.674$ and $\sigma T_{nb}^4 = 0.658$								

Clockwise

0	0.523	0.523	0.676	0.658	0.541	0.541	1.000	1.000
10	0.523	0.520	0.676	0.658	0.538	0.541	0.994	0.985
20	0.524	0.488	0.675	0.659	0.504	0.542	0.930	0.940
30	0.520	0.450	0.674	0.659	0.465	0.538	0.864	0.866
40	0.517	0.388	0.674	0.660	0.402	0.535	0.751	0.766
50	0.517	0.322	0.673	0.660	0.335	0.535	0.626	0.643
60	0.517	0.251	0.671	0.661	0.261	0.535	0.488	0.500
70	0.516	0.174	0.669	0.661	0.182	0.534	0.341	0.342
80	0.515	0.075	0.667	0.662	0.080	0.533	0.150	0.174
90	0.515	0.000	0.662	0.662	0.000	0.533	0.000	0.000
$\sigma T_n^4 = 0.676$ and $\sigma T_{nb}^4 = 0.658$								

TABLE X

COSINE RESPONSE TEST DATA: ROTATION ABOUT AXIS C-C
(Note: Subscript "b" refers to background flux)

Counterclockwise

Angle of Incidence ϕ°	Thermopile Output at Normal Incidence (K_n) $K_n = (K'_n - K_{nb})$	Thermopile Output at ϕ° Incidence (K_ϕ) $K_\phi = (K'_\phi - K_{\phi b})$	σT_ϕ^4	$\sigma T_{\phi b}^4$	$G_1 = K_\phi + \sigma(T_\phi^4 - T_{\phi b}^4)$	$G_2 = K_n + \sigma(T_n^4 - T_{nb}^4)$	$G_1 \div G_2$	$\cos \phi$
0 normal	0.560	0.560	0.676	0.665	0.571	0.571	1.000	1.000
10	0.560	0.552	0.676	0.665	0.563	0.571	0.986	0.985
20	0.560	0.530	0.675	0.665	0.540	0.571	0.946	0.940
30	0.560	0.489	0.675	0.666	0.498	0.571	0.872	0.866
40	0.559	0.435	0.673	0.666	0.442	0.570	0.775	0.766
50	0.559	0.367	0.671	0.666	0.372	0.570	0.653	0.643
60	0.559	0.282	0.670	0.666	0.286	0.570	0.502	0.500
70	0.559	0.198	0.666	0.666	0.198	0.570	0.347	0.342
80	0.559	0.094	0.662	0.666	0.090	0.570	0.158	0.174
90	0.559	0.000	0.662	0.662	0.000	0.570	0.000	0.000
$\sigma T_n^4 = 0.676$ and $\sigma T_{nb}^4 = 0.665$								

Clockwise

0	0.560	0.560	0.678	0.660	0.578	0.578	1.000	1.000
10	0.560	0.543	0.676	0.660	0.559	0.578	0.967	0.985
20	0.570	0.526	0.676	0.662	0.540	0.588	0.918	0.940
30	0.565	0.488	0.676	0.662	0.502	0.583	0.861	0.866
40	0.565	0.424	0.674	0.662	0.436	0.583	0.748	0.766
50	0.568	0.360	0.672	0.662	0.370	0.586	0.631	0.643
60	0.565	0.277	0.670	0.661	0.286	0.583	0.491	0.500
70	0.565	0.190	0.666	0.662	0.194	0.583	0.333	0.342
80	0.565	0.092	0.662	0.660	0.094	0.583	0.161	0.174
90	0.561	0.000	0.660	0.660	0.000	0.579	0.000	0.000
$\sigma T_n^4 = 0.678$ and $\sigma T_{nb}^4 = 0.660$								

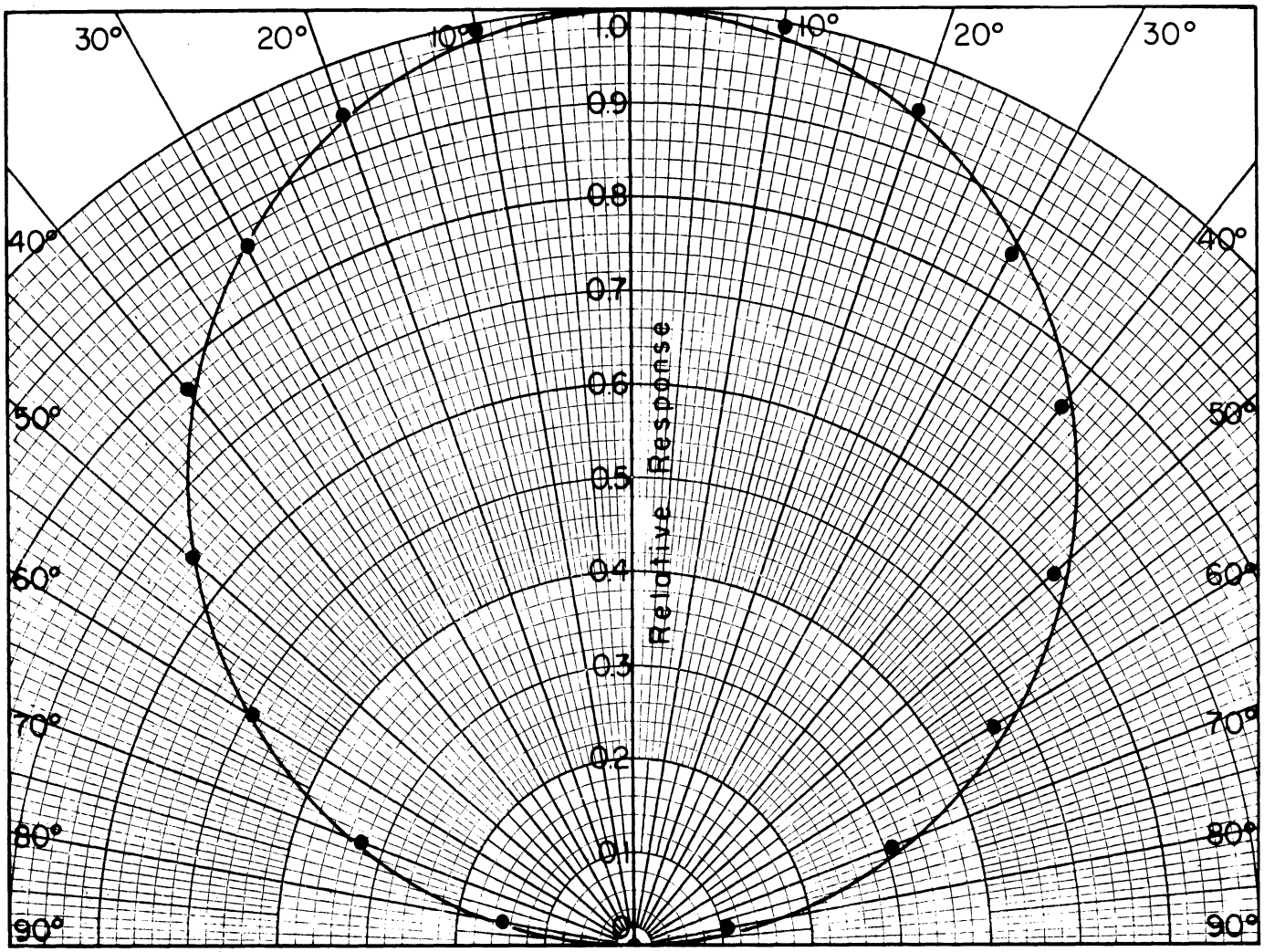

Fig. 6

COSINE RESPONSE
OF
BECKMAN & WHITLEY
TOTAL HEMISPHERICAL RADIOMETER

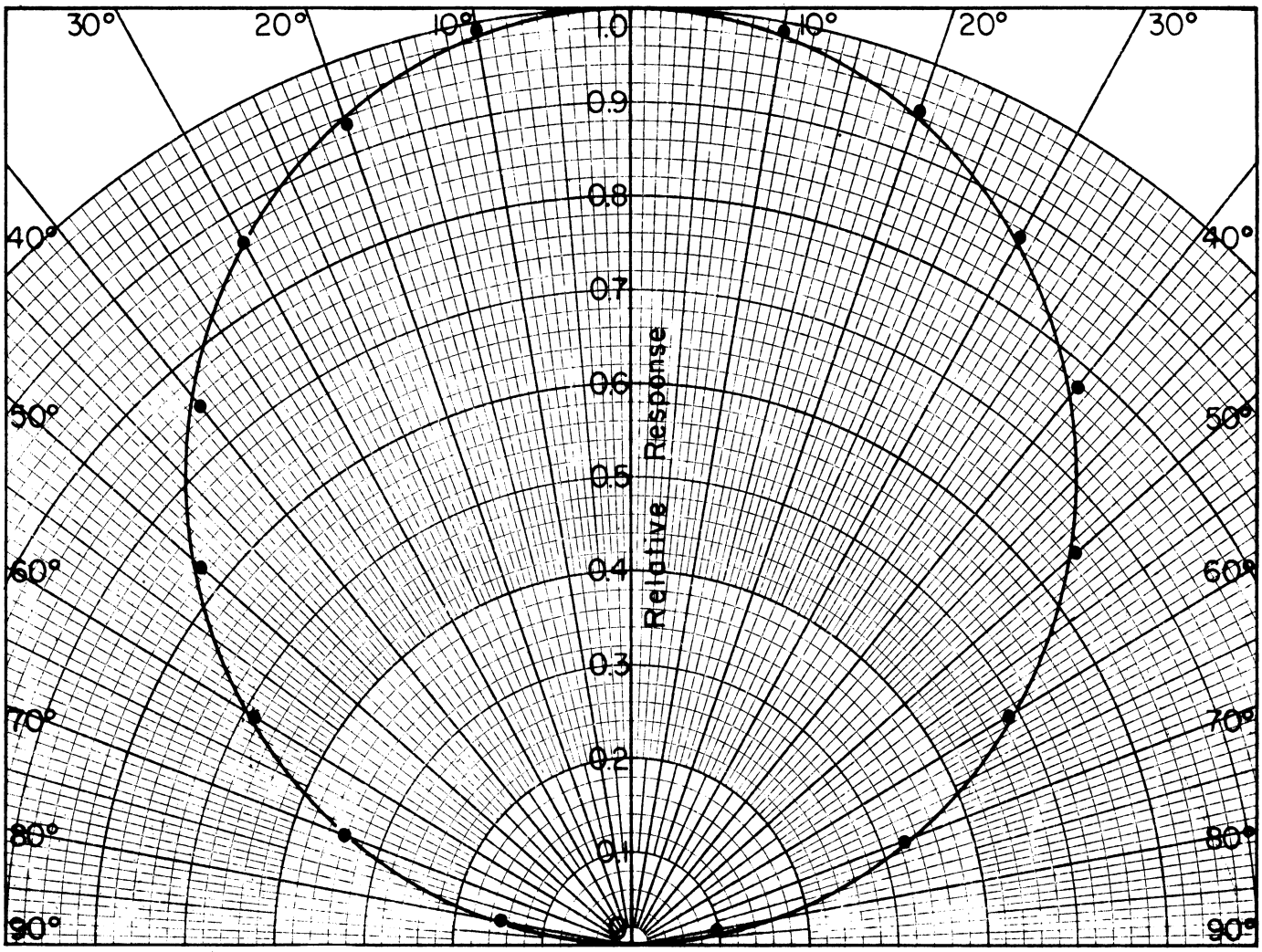

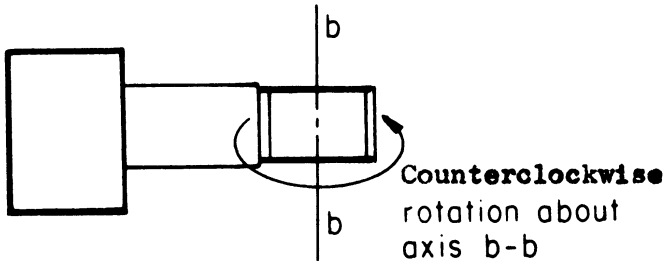

Fig 7

COSINE RESPONSE

OF

BECKMAN & WHITLEY

TOTAL HEMISPHERICAL RADIOMETER

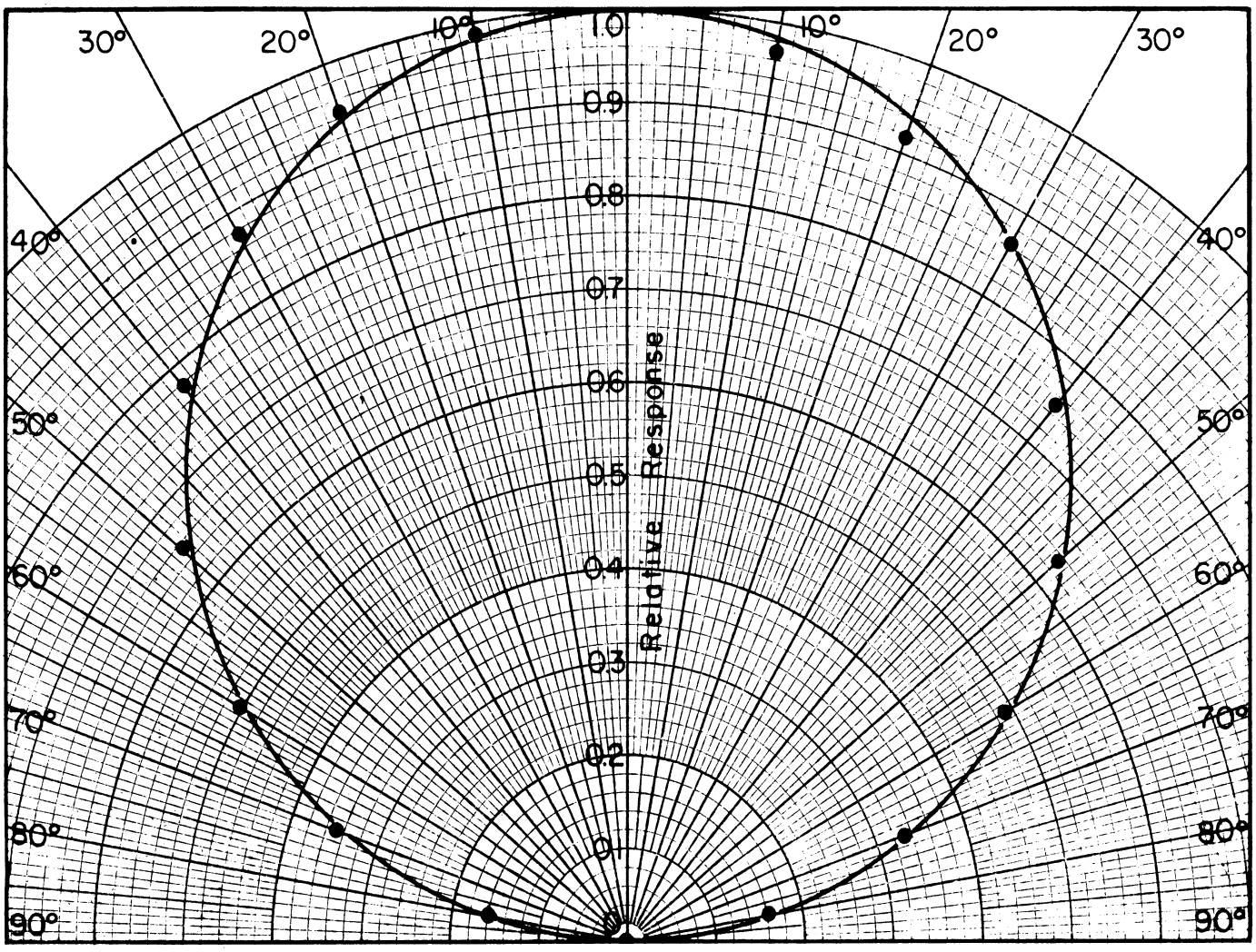

Fig. 8
COSINE RESPONSE
OF
BECKMAN & WHITLEY
TOTAL HEMISPHERICAL RADIOMETER

APPENDIX A

Equipment and Procedures for Wind Tunnel Tests

A. Equipment

The radiometer was tested in a low speed wind tunnel which has a 14' x 8' x 5.5' working section. The tunnel is a closed loop, double return, type with a contraction ratio of approximately 4 to 1 at the Venturi section. The air is circulated by an adjustable-pitch, axial flow fan powered by a variable speed d.c. motor. Air speed in the tunnel is measured by a pitot tube and a micro-manometer.

Figure 9 is a sketch showing the opposing wind test position of the radiometer in the wind tunnel working section. It shows also the arrangement of three apertures for admitting the radiation flux. Figure 11 shows the radiometer in the left cross wind test position. The radiometer support had leveling screws and an arrangement for height adjustment.

The source of radiation was a 250 watt Westinghouse Reflector Infrared Heat Lamp mounted an inch above the topmost aperture. A series of temperature measurements established that this arrangement of heat lamp and apertures provided steady temperatures independent of tunnel air speed for both the lamp and the wind tunnel ceiling surrounding the lower-most aperture. An arrangement such as this was found necessary when it was observed that a glass window through which radiation was admitted changed temperature with change in wind speed. A smoke tracer test indicated that air entering the tunnel through the aperture did not penetrate the main air stream more than 6 inches from the tunnel ceiling before leaving the working section.

Alternating current was supplied to the heat lamp through a circuit including an ammeter, a voltmeter and a Variac. The circuit arrangement is shown in Figure 10 and the meters and Variac are shown in Figure 12.

The radiometer thermopile output was recorded on a Brown recording potentiometer with a range of 0 to 12 millivolts. The thermocouple junction imbedded in the sensing element and an additional junction positioned at the intake of the radiometer blower motor could be alternately connected to a reference junction maintained in a zero degree C. ice bath. The thermocouple outputs were recorded with a Leeds and Northrup, Adjustable-Zero-Adjustable-Range (AZAR), recording potentiometer. A one millivolt range was used. Wiring diagrams are shown in Figure 10 and the recorders are shown in Figure 12.

B. Procedures

For each orientation of the radiometer the thermopile and thermocouple outputs were recorded with the heat lamp on and the tunnel motor off until steady conditions prevailed for both radiation flux and sensing element and

air stream temperatures. The tunnel blower motor was then started and operated at various selected speeds for periods of five minutes or more at each speed. To cover the range of 5 to 50 mph it was necessary to use two pitch settings of the fan blades.

An observer continuously monitored the power supply to the heat lamp and adjusted the Variac whenever necessary to maintain constant power. He also switched from sensing element thermo-junction to air intake thermo-junction for each steady speed interval. After a series of speed runs the tunnel motor was stopped and a steady "no wind" reading was obtained.

The wind tunnel test data are given in Tables I, II, III and IV.

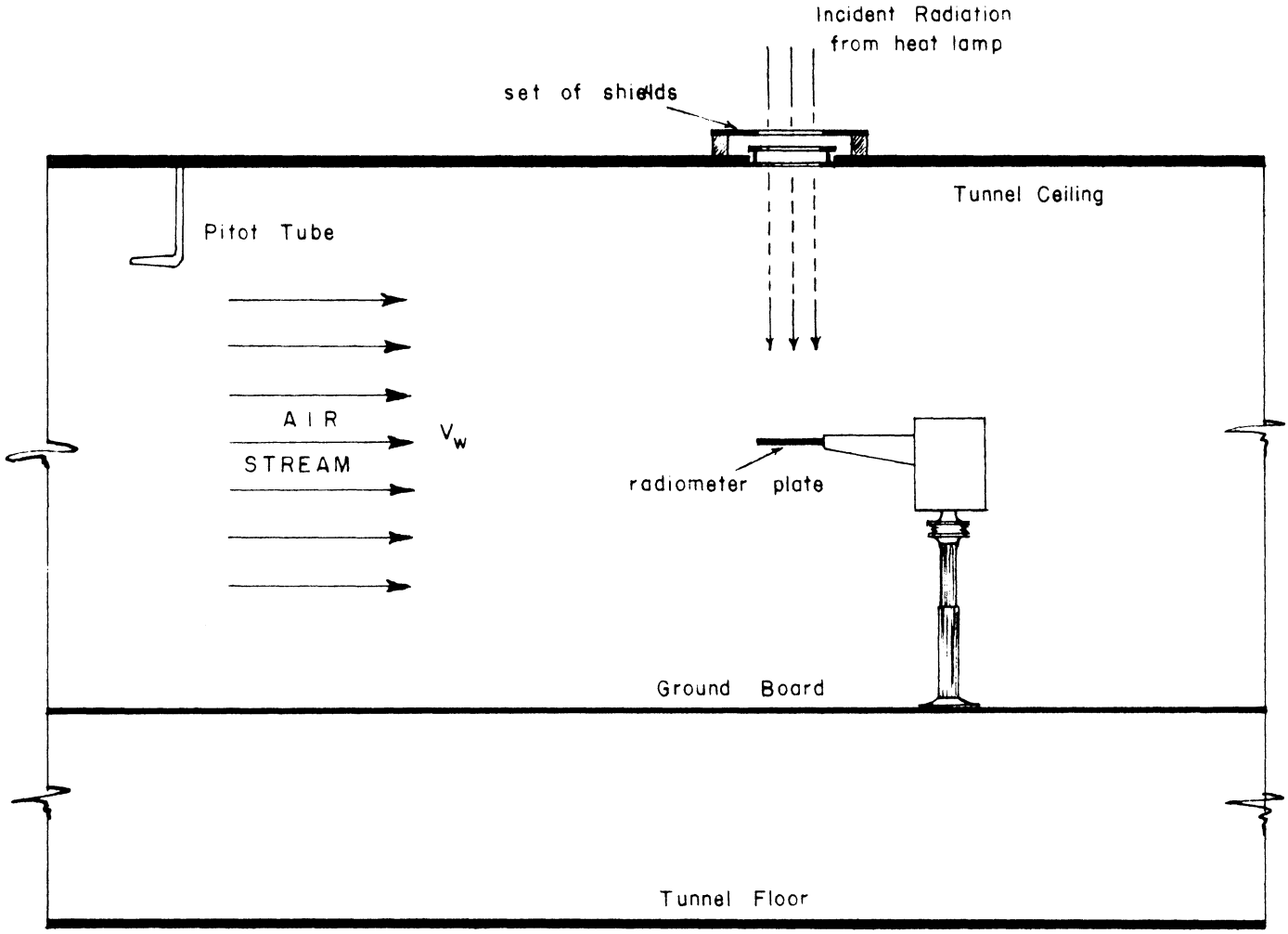

FIGURE 9 SECTIONAL ELEVATION OF WORKING SECTION OF WIND TUNNEL SHOWING RADIOMETER IN TESTING POSITION

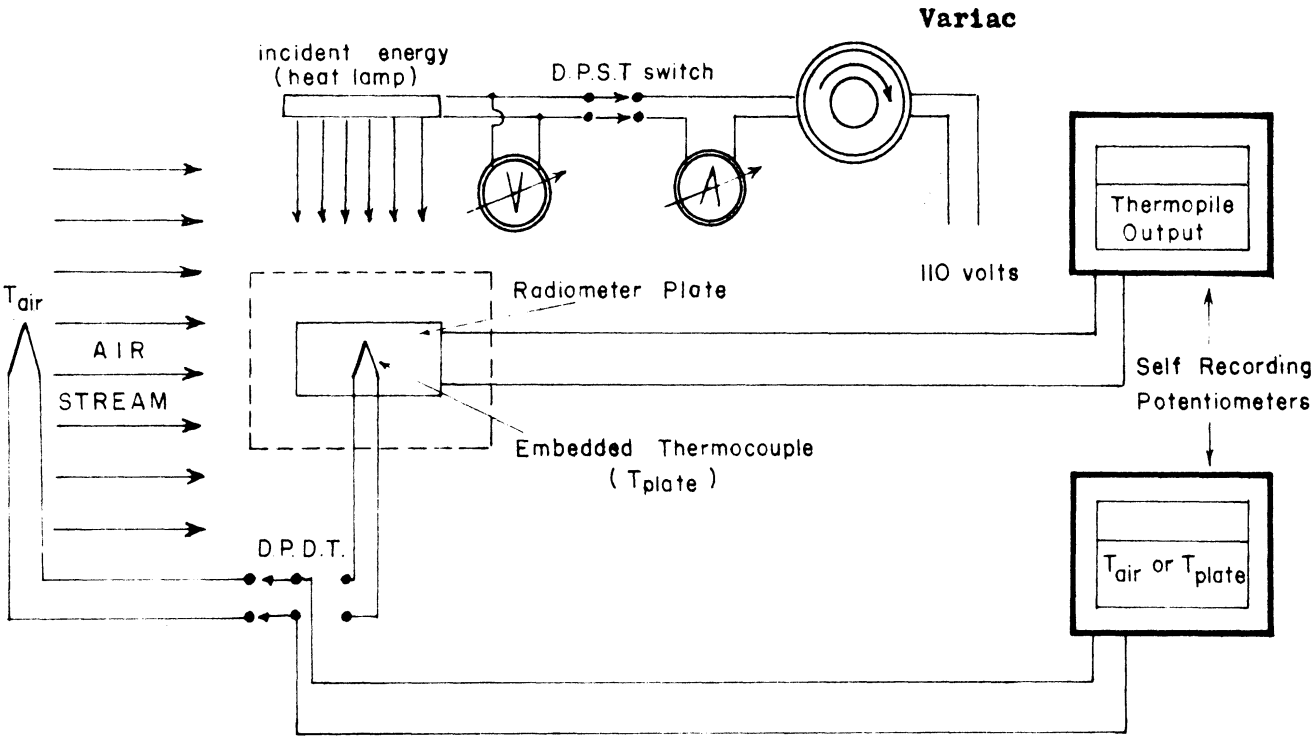

FIGURE 10 ELECTRICAL WIRING DIAGRAM FOR MEASUREMENT OF RADIOMETER RESPONSE

APPENDIX B

Equipment and Procedures for Natural Wind Tests

To test the influence of natural wind on the performance of the total hemispherical radiometer a field experiment was conducted at the Willow Run Micrometeorological Field Station. The field station is on the eastern edge of the Willow Run Airport in such a position that air moving over the station from the NNW, through west, to SSW passes over a nearly uniform flat and level surface for a distance of more than a mile. During the tests the surface cover at the field station was grass which was cut to 5 to 8 cm in height. The grass extended westward from the field station a few hundred feet and the remainder of the airport was covered with short grass or grain stubble. The data reported in Table V were obtained with a southwest wind.

A. Equipment

The radiometer was mounted on a pedestal formed by a 2" gas pipe with the sensing element horizontal and about 1 meter from the ground. A Beckman and Whitley Model 170-34 Wind Speed Transmitter was mounted about 2.5 meters north of the radiometer and at the same height. A Beckman and Whitley Model 170-53 Wind Direction Transmitter was located 2.5 meters north of the wind speed transmitter. An Eppley pyrheliometer was mounted on the top of a van housing recorders and located about 20 meters northeast of the radiometer. A mast supporting four shielded, fine-wire thermocouple junctions was located about 30 meters southeast of the radiometer.

The output of the radiometer thermopile was recorded on a Leeds and Northrup AZAR (continuous line-drawing) recorder with a full-scale range setting of 15.6 millivolts. The chart speed was 0.25 inches per minute. Zero degree C. ice baths were maintained for reference junctions for both the radiometer thermocouple junction and the air temperature junctions. Thermocouple and pyrheliometer outputs were programed on a 0 to 4 miltivolt range multipoint Leeds and Northrup recorder. The chart speed of the multipoint recorder was 0.40 inches per minute.

The wind speed and direction transmitter outputs were recorded on Esterline-Augus milliameter recorders having 0-1 ma ranges. The chart drives were operated at 0.75 inches per minute. All recorders were equipped with shorting switches so that the recordings could be synchronized by simultaneously switching them to "zero check."

B. Procedures

In order to obtain the three different radiometer positions with respect to wind direction, the radiometer was oriented by eye with respect to the wind vane while the latter was held in a position representing the average direction indicated by the preceeding recording. The wind direction recorder was operated during the orientation to obtain a reference direction. All the recorders were operated simultaneously, then, for each of the periods listed in Table V.

APPENDIX C

Equipment and Procedures for Cosine Response Tests

A. Equipment

The cosine response tests were conducted in a large subterranean photometric laboratory. The room had no windows and its interior walls and fittings were black. It was nearly an ideal location for the tests since there were no stray radiations by reflection and the entire room remained at nearly constant temperature regardless of weather or time of day. Automatically controlled voltage was available for the radiation source.

Figure 13 (a) is a sketch of the basic arrangement of radiation source, shutter, apertures and radiometer. The radiation source, an RSP-2 Ken Rad Photo Spot Lamp, was about 1 meter from the shutter and the radiometer was about 1.5 meters from the aperture nearest it. The radiometer was mounted on the base of a Warner and Swasey Azimuth Instrument which could be set to a precision of about 0.01 degrees. Radiometer mountings for rotations about axes b-b and a-a are shown in Figures 14 and 15, respectively.

To assist in aligning the radiometer for normal incidence exposure, a photo-electric device was constructed and attached to the radiometer mounting. It consisted of a narrow tube with a small aperture at one end and a barrier type photocell at the other. The tube was arranged normal to the radiometer sensing element in such a way that a small deviation from normal incidence produced a large change in photo-electric output as indicated on a sensitive, portable galvanometer. The galvanometer and the photo-electric device attached to the structure supporting the radiometer are shown in Figure 14.

The recorders used for these tests were the same as those used in the wind tunnel tests. They are described in Appendix A.

B. Procedures

The test procedure consisted of obtaining steady recordings of the thermopile and thermocouple outputs for each angular position. Two recordings were made for each position, one with the shutter open and one with the shutter closed. The difference between the two gives the radiant flux from the lamp alone if the small area of the shutter can be neglected with respect to the total background. The differences were used to compute deviations from the cosine law as indicated in Tables VIII, IX and X. Normal incidence measurements were made at frequent intervals.

(a)

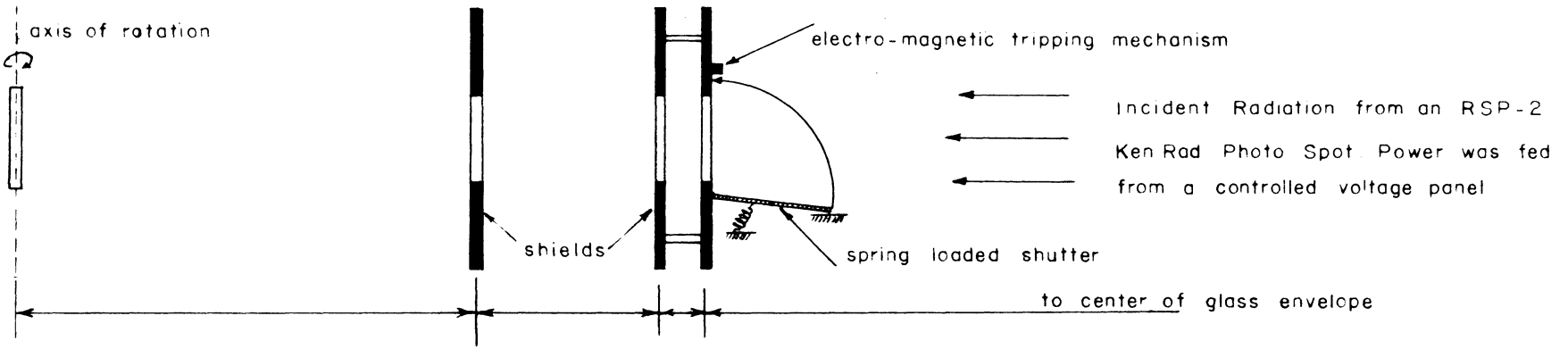

Figure 13 Equipment used for testing the Transient Response and Cosine Response of total hemispherical radiometer

(b)

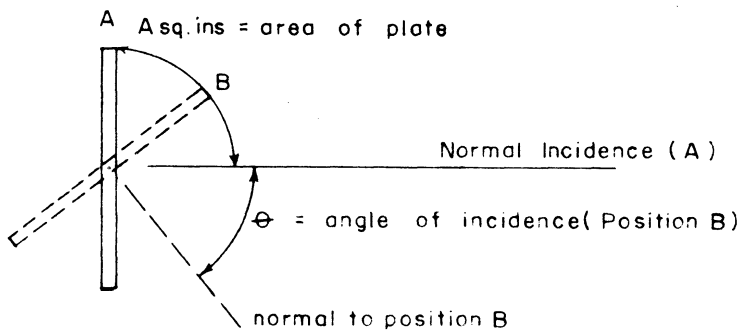

A is position for normal incidence

B " " θ° "

Note : Rotation of the sensing plate changes the angle of incidence. If the cosine law is obeyed, then the response should be proportional to the area intercepted by the plate for θ° rotation. For θ° rotation the projected area is Acos θ , hence the net radiation on the plate is proportional to cosine of θ

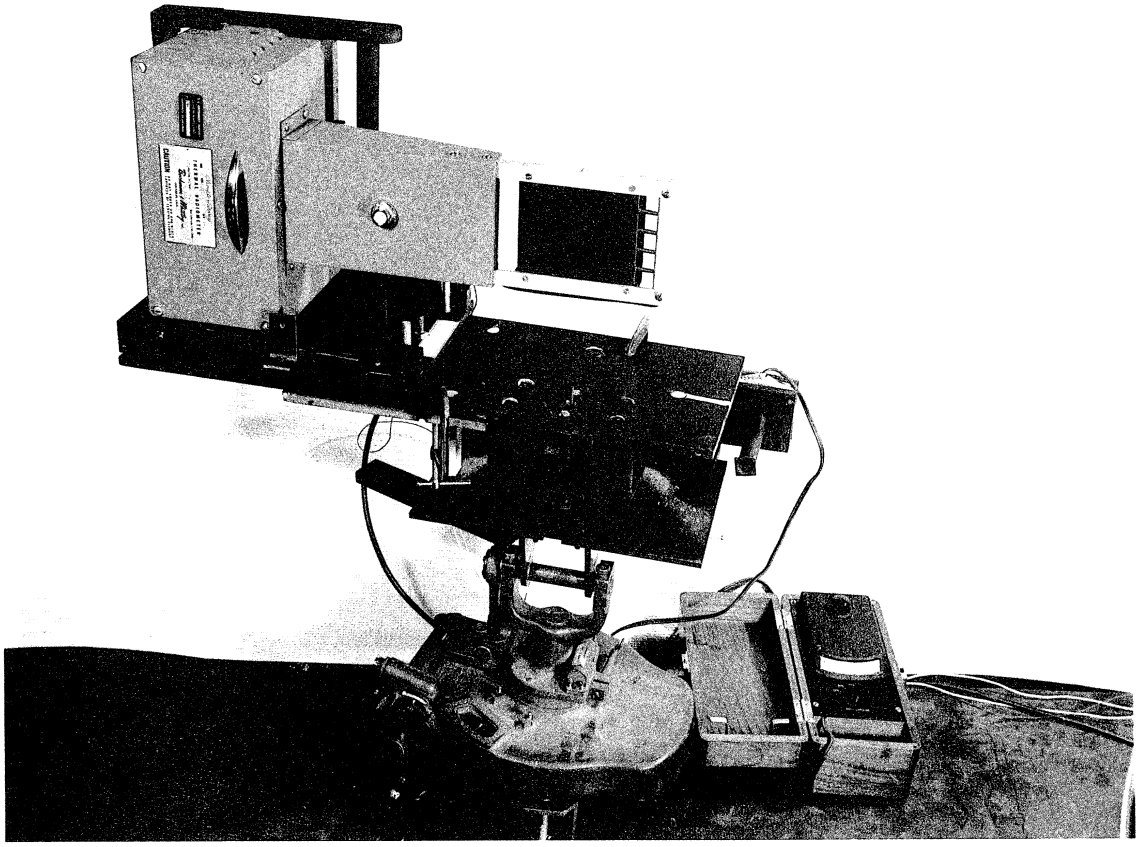

Figure 14. View of Radiometer Mounting for Cosine Response Test: Rotation about Axis b-b.

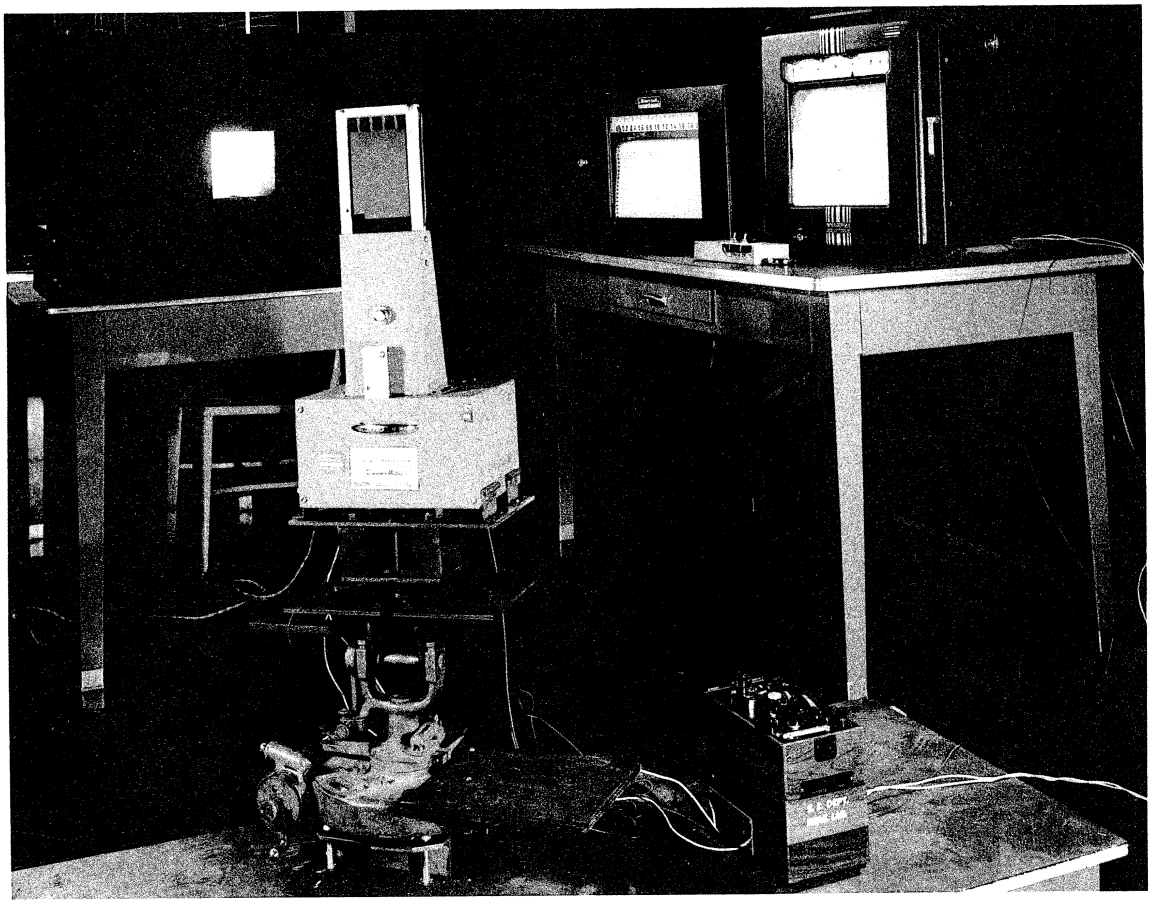

Figure 15. View of Radiometer Mounting for Cosine Response Test: Rotation about Axis a-a.

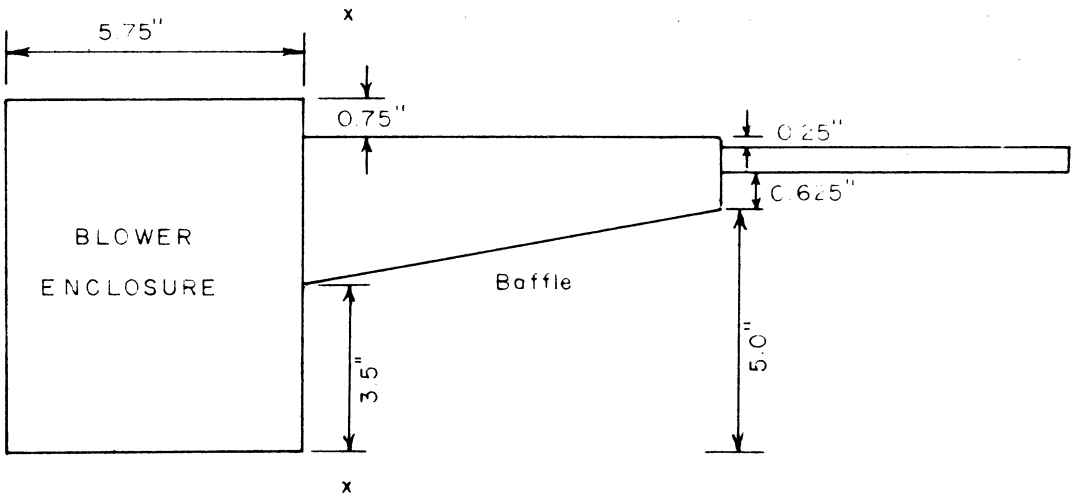

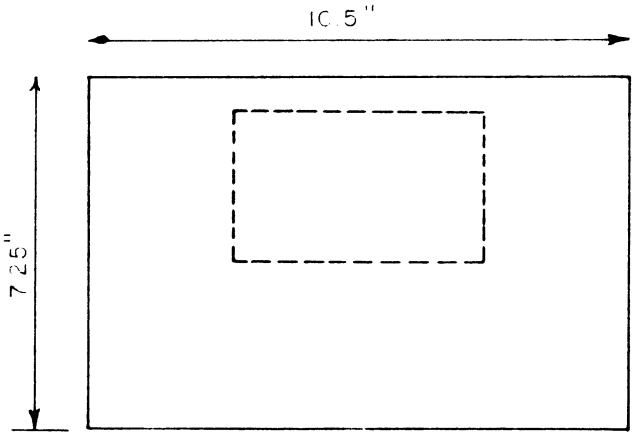

section x-x

Blower Inlet

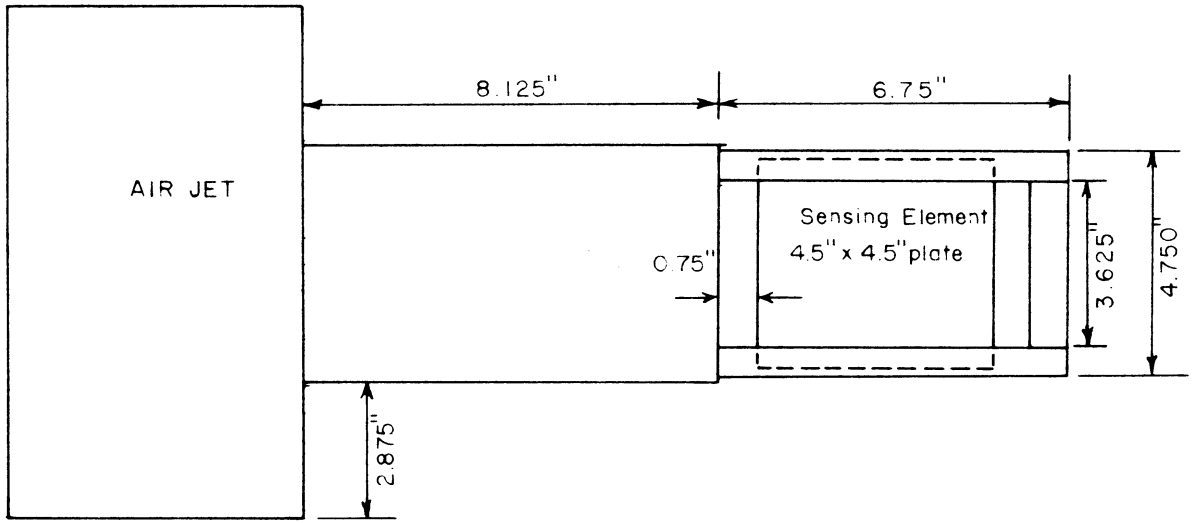

- SPECIFICATIONS -

Sensitivity	10 Millivolts / ly /min.
Internal Resistance	440 Ohms
Response Time	12 seconds
Reference Thermocouple	Copper - Constantan
Air Flow	50 c.f.m
Blower Motor	115 v 60 cps

Figure 16 Overall Dimensions of Total Hemispherical Radiometer

REFERENCES

1. University of California, Department of Engineering, Division of Engineering Research, Non-Selective Radiometers for Hemispherical Irradiation and Net Radiation Interchange Measurements, Report No. 9, Report Code NR-015-202, October 1949.

2. Parekh, Natwar M., Heat Transfer Coefficients from Short Flat Plates--the Influence of R_e, Leading Edge Shape and Angle of Attack, Stanford University, May 1948.

3. Fuquay, Don, and Buettner, Konrad, "Laboratory Investigation of Some Characteristics of the Eppley Pyrheliometer," Trans. Amer. Geophys. Union, 38, 38-43 (1947).